ARTICLE

Human Blood Investigation of Ta-Coated 316L Stainless Steel to Evaluate Corrosion and Wear Behaviour Against Other Artificial Fluids for Orthopaedic Implants

Dileep Pathote[1] | Ashwani Ranjan[2] | Abhijit Mandal[3] | Sandeep Kumar[4] | R. K. Gautam[2] | C. K. Behera[1]

[1]Department of Metallurgical Engineering, IIT (BHU), Varanasi, India | [2]Department of Mechanical Engineering, IIT (BHU), Varanasi, India | [3]Department of Radiotherapy and Radiation Medicine, Institute of Medical Science, Banaras Hindu University, Varanasi, India | [4]Department of Pathology, Institute of Medical Science, Banaras Hindu University, Varanasi, India

Correspondence: Dileep Pathote (dileeppathote.rs.met20@iitbhu.ac.in)

Received: 14 November 2024 | **Accepted:** 7 February 2025

Funding: The study was supported by the India's Science and Engineering Research Board (SERB) under Project No. R&D/SERB/MET/19-20/04.

Keywords: 316L stainless steel | electrochemical corrosion | human implants | metallic coating

ABSTRACT

Stainless steel (316L) is widely used in biomedical applications, but concerns persist regarding its long-term surface properties, particularly in varying patient environments over time. This study aims to enhance the surface properties of 316L stainless steel through a 1.504 μm tantalum (Ta) coating applied via DC magnetron sputtering. The corrosion and wear behaviours were evaluated in different mediums, including human blood (HB), artificial saliva (AS), Ringer's solution (RS), and simulated body fluid (SBF). The Ta-coated 316L SS exhibited a shift toward nobler corrosion behaviour, with a corrosion rate of 0.146×10^{-2} mm/year in human blood, compared to the uncoated 316L SS, which showed corrosion rates of 0.325, 0.556, 0.779, and 1.425×10^{-2} mm/year in HB, RS, AS, and SBF, respectively. Electrochemical impedance spectroscopy (EIS) results indicated higher corrosion resistance of Ta-coated 316L SS in human blood than in other fluids. Potentiodynamic polarisation (PDP) results reveal that corrosion rate and current increased as the fluid environment shifted from human blood to simulated body fluid. Wear tests further demonstrated the superior wear resistance of the Ta-coated 316L SS, with a minimum wear rate of 0.086×10^{-5} mm^3/Nm, compared to the uncoated 316L SS, which exhibited a maximum wear rate of 0.25×10^{-5} mm^3/Nm. The microstructural analysis confirmed significant improvements in the surface properties of Ta-coated 316L SS, particularly in the human blood environment.

1 | Introduction

316L Stainless steel is a modified series of low-carbon Cr–Mo–Ni austenitic stainless steel. Its main components include molybdenum (Mo) (2%–3%), chromium (between 16% and 18%), nickel (Ni) (10%–12%), silicon (< 1%), sulphur, phosphorus, and iron (Fe) are also present. Grade 316L is often employed in process streams containing chlorides or halides [1]. Adding Mo provides resilience to corrosion concerning the local attack of chloride corrosion and corrosion by reducing acids. Grade 316L stainless steel contains less carbon than grade 316 stainless steel. When freezing, the 316L stainless steel can produce high yields and strong power, like Duplex's flawless markings. Grade 316L also offers a high-rise, low-to-crack, and strong strength at high temperatures [2]. In addition to excellent resilience to corrosion and power structures, 316L Cr–Mo–Ni grade alloys also perform better [3]. In recent years, it has been noticed that the list of applications for 316L SS is endless. It is commonly employed in the petrochemical, chemical, food processing, pharmaceutical, and medical

equipment industries [4]. In medicine, Austenitic stainless steel is the most often employed stainless steel (AISI 316L) because it has acceptable biological compatibility, excellent performance properties, and the proper density for load-bearing functions, thus making this an appealing surgical implant [5]. Implant materials are subjected to complex environments that can significantly impact their corrosion and wear resistance, which are crucial factors in implant longevity and biocompatibility. Corrosion resistance directly affects metal ion release, influencing the body's inflammatory response and compromising implant stability over time. Wear behaviour, particularly in load-bearing applications, can lead to mechanical degradation and the formation of wear particles, further exacerbating corrosion. To assess these behaviours comprehensively, various body fluids such as artificial saliva (AS), Ringer's solution (RS), and simulated body fluid (SBF) are commonly used as test media [4–6].

Metallic biomaterials have a higher strength, fatigue, and fracture strength than polymeric and ceramic materials [6]. An essential requirement for selecting any implant material is that it must possess good biocompatibility. Alloys and metals are widely employed in various ways, such as fittings, which give the necessary mechanical endurance, corrosion resilience, and high biocompatibility [7]. Several metallic biomaterials are employed as bone grafts. In contrast, stainless steel is widely used for its main advantages of low cost, good mechanical characteristics, simple processing, good corrosion resilience, and widespread availability [8].

Stainless steel (316L) is the most prevalent material for biomedical applications, per the literature review. However, it has been pointed out that Ni in stainless steel causes several allergic reactions in the human body. Because of the toxicity of Ni in the human body, efforts are being made to develop austenitic stainless steels without Ni or low Ni for biomedical use [9–16]. Corrosion pit is a different sort of anodic reaction, and It's a self-catalytic reaction [17].

The most often utilised materials for bone and dental implants are austenitic stainless steel, particularly AISI316L stainless steel. This is due to its superior biomechanical qualities, low cost, ease of production, and welding compared to other metals like Co–Cr and Ti and their alloys. However, if employed for a long time, AISI 316L SS has some problems, including cytotoxicity from the release of poisonous ions, local corrosion, and ageing, which make it unsuitable for use in biological environments. The literature shows increased Fe^{+2}, Cr^{+3}, and Ni^{+} ion concentrations in the human body can substantially impair muscular function, leading to allergies and inflammation [18]. The immune system might also divide and reject the outer body as an alternative. Biocompatibility is thus heavily dependent on the object's surface area and resilience to metallic biomaterial corrosion. The tantalum (Ta)-based films are considered good choices because of their strong molecular strength and resilience to high electrochemical stability. Transformation is an appealing solution for increasing biocompatibility and resilience to metallic biomaterial corrosion. Ta-based films are attractive alternatives because of their high molecular performance and electrochemical stability [19].

Ta film can significantly enhance the radiopacity of the NiTi-based alloy if ta-based films are used to treat metallic biomaterials and improve their biological adhesion. Furthermore, when 96% Ni^{2+} was reduced from Ta-coated NiTi alloy, the sample was less than the amount of unbleached NiTi alloy, and they discovered that Ta films successfully reduced Ni^{2+} extraction [20]. Considering the benefits of Ta and Ta-based films integrated into 316L SS, a plasma-assisted chemical vapour deposition pulsed-DC plasma process improves vapour permeability, corrosion resilience, and biocompatibility [21].

Studies [22] on 21 days of immersion in abiotic saliva, high-nitrogen stainless steel (HNS) alloys with nitrogen contents of 0.88 wt.% and 1.08 wt.% exhibited significantly reduced hole depth compared to 316L stainless steel, indicating better resistance to pitting corrosion. When exposed to *Streptococcus mutans* biofilms, 316L stainless steel showed a higher corrosion rate (CR) than HNS alloys. Cytotoxicity testing with MC3T3-E1 pre-osteoblast cells demonstrated that HNS alloys were nontoxic, supporting better sessile cell development than 316L stainless steel. This suggests that HNS alloys provide a favourable environment for cell growth, enhancing their potential for biomedical applications [22–25]. As per the [26], Hydroxyapatite $Ca_{10}(PO_4)_6(OH)_2$ is a bioactive ceramic and biocompatible that is widely used for coating implant surfaces to improve their biocompatibility and osseointegration. However, HA is brittle and has low mechanical strength, which makes it unsuitable for direct use in implant devices. Therefore, the development of HA coatings (HAC) and composites is an active area of research. According to the [27], The concentration of chromium (Cr) and Mo in the passive film decreases with increasing pH and sputtering depth while the concentration of Fe increases. This is due to Cr oxides' higher thermodynamic stability than iron oxides. However, at elevated pH levels, a decrease in Cr and Mo concentration contributes to the degradation of the passive oxide film, reducing corrosion resistance. In this study, SBF was used to evaluate the corrosion resistance of titanium-reinforced 316L stainless steel. While extensive research is on the biocompatibility of stainless-steel alloys, advanced methodologies are required to gain deeper insights into the biocompatibility of metals alloyed with additional elements. Such insights are crucial for optimising anticorrosion properties and promoting osteointegration in biomedical applications [28–30].

Although numerous studies have focused on metallic coatings for enhancing the corrosion resistance of 316L stainless steel, there is a notable lack of research specifically addressing pure Ta coatings on 316L SS in biological environments, particularly in human blood. Furthermore, studies that employ human blood as a testing medium for these coatings have not been studied yet, leaving a gap in understanding the behaviour of Ta-coated 316L SS under physiologically relevant conditions. This study is the first to evaluate the electrochemical corrosion and wear behaviour of a pure Ta coating (1.504 μm thickness) on 316L stainless steel in human blood (B-positive), alongside AS, RS and SBF. Using the DC magnetron sputtering technique to deposit the Ta coating, we characterised the coated and uncoated 316L SS samples using advanced techniques such as optical microscopy, scanning electron microscopy (SEM), energy-dispersive X-ray spectroscopy (EDS), and X-ray diffraction (XRD) both before and after corrosion testing. This research aims to establish Ta-coated 316L SS as a candidate

biomaterial with enhanced durability, corrosion resistance, and suitability for human implant applications by providing critical insights into its performance in human blood and simulated bodily environments.

2 | Experimental Details

2.1 | Materials and Sample Preparation

Austenitic stainless steel 316L with dimensions of $472 \times 775 \times 20$ mm was supplied by Mishra Dhatu Nigam Limited (MIDHANI) in Hyderabad, India. The received chemical composition is typically shown in Table 1. Using the 316L SS as received, a table-moving CNC wire-cut EDM machine formed the necessary samples, sized $20 \times 20 \times 2$ mm. Silicon carbide waterproof paper was employed to polish all the samples up to 1600 grit. The final polishing was done with a 3-micron diamond paste to achieve a polished surface. Cleaning was done in acetone for 10 min before being rinsed and dried in deionised water. The microstructure of SS 316L (except Ta-coated) is reveal by using Aqua regia, a solution made by mixing nitric acid and hydrochloric acid in a 1:3 molar ratio, as an etchant.

2.2 | Ta Coating

To deposit the thin film onto stainless steel 316L, a high-purity sputter Ta target of 99.95% Ta with a diameter of 55.8 mm and a thickness of 3.175 mm was utilised. The Ta target was acquired from M/S Indo French High Tech Equipments in Mumbai (India) and used with a DC magnetron Sputtering system (Vacuum Industries Ltd., Peenya Bengaluru, India). Before coating, the substrates were cleaned using an ultrasonic cleaner, acetone and distilled water. Compressed air was then used to dry the surfaces. The description of the physical vapour deposition (PVD) coating process was adopted [31]. Table 2 displays the DC magnetron sputtering operational parameters for the coating process. Before the deposition process, an ultrasonic cleaner was used to clean the sample. Acetone was used in the cleaning process, and then pure Argon (Ag) gas flow was used for drying. The sample was exposed to a deposition time of 15 min. During the DC magnetron sputtering, 316L SS substrates were placed directly underneath the target's tracks. Before beginning each layer deposition process, the targets' surfaces were thoroughly cleansed of all contaminants and impurities for 15 min. The gas flow was controlled by a mass flow controller (MFC). The chamber was evacuated to a 5×10^{-4} Pa base pressure before deposition.

2.3 | Microstructure

Initially, all the samples of 316L SS surface were analysed for their experimental morphology by an optical microscope (LeicaZ6 APO on OM) and SEM (ZEISS MA 15/18 and UK). Subsequently, the sample was coated with Ta for 15 min. by a DC sputtering machine on 316L SS. A sample was investigated to capture morphological features on the surface using SEM, and the chemical analysis of the sample was done using EDS. They were analysed with a PANalytical X-Pert Pro MPD diffractometer (Rigaku Smart Lab 9 kW Powder type without χ cradle, RIGAKU Corporation), with a voltage of 45 kV, a current of 30 mA, and a step of 0.01 02°/s the materials were investigated by XRD using Cu K radiation. A PANalytical X-Pert MRD- θ-2θ at 45 kV and 20 mA with an offset angle of 7° and penetration depth of an estimated 250 nm was also used to conduct grazing incidence XRD measurements.

2.4 | Electrochemical Corrosion

Open circuit potential (OCP), potentiodynamic polarisation (PDP), and electrochemical impedance spectroscopy (EIS) tests were employed to characterise electrochemical measurements. The human blood of approximately 300 mL packed blood red cells (PRBC human blood, B^+) was collected from the Blood Centre, Institute of Medical Sciences, Banaras Hindu University, Varanasi, India. This was left over until the expiration date. The blood was preserved in citrate-phosphate-dextrose-adenine (CPDA), quite cognisant with saline, adenine, glucose, and manitol (SAGM) additive to increase the cell life, and the remaining blood after the test was discarded as per protocol. The high purity of chemicals (Alpha Assar-AR grade) for AS, RS, and SBF are given in Tables 3a–d. In the typical three-electrode system, the working electrode is 316L stainless steel, the reference electrode is Ag/AgCl, and the counter electrode is platinum wire, employed in electrochemical corrosion measurement. Supporting Information: Figure S1 Schematic pictorial view of Electrochemical corrosion test setup in human blood depicts electrochemical corrosion test setup and human blood used in this study. The EIS measurements were performed for all coated and uncoated samples by varying the frequency from 100 K Hz to 0. The sampling frequency was set at 1 Hz with an amplitude of 10 mV logarithmic for the excitation signal. Electrochemical tests, including PDP, were conducted at a scan rate of 0.2 mV/s. The human blood had a pH of 7.2, and the AS, ringer, and Simulated body fluid pH were (7.39, 7.19, and 7.26, respectively) with ±0.11 at 37°C. The working electrode was exposed to 1 cm^2 using the CS2350 corrtest potentiodynamic apparatus.

2.5 | Wear Studies

To conduct wear studies, a $20 \times 20 \times 2$ mm 316L stainless steel sample was prepared by grinding and subsequently polished using emery paper with grades of up to 1600. This polishing and 30-min ultrasonication treatment resulted in a smooth, scratch-free mirror surface. Following this preparation, a Ta coating was applied to the stainless steel using a DC Magnetron Sputtering (DCMS) system.

TABLE 1 | The chemical composition of received 316L stainless steel (wt.%).

Material	Ni	Mn	Cr	Mo	C	P	S	Si	Fe
316L SS	13.6	1.39	17.5	2.27	0.03	0.003	0.005	0.015	Balanced

TABLE 2 | DC magnetron sputtering operational parameters for the coating procedure.

Parameters	Details	Reason
Target material	Tantalum	Tantalum films can exist in two different crystalline phases: α-phase and β-phase. The α-phase is the more stable and has a body-centred cubic crystal structure, while the β-phase has a hexagonal close-packed crystal structure toughness and good corrosion resistance [16].
Magnetron source	02 Nos. (50.8 mm each)	A source shutter pre-ionises the material to be deposited and shields the cathode from cross-contamination.
Special magnetics	—	To provide uniform sputtering.
Gas	Argon (Ar)	It can play a significant role in the PVD process and can be used to optimise the coating's nucleation density and surface roughness.
Working temperature	180°C	The capability of producing thin compounds with controlled stoichiometry, composition, and high deposition rate.
Voltage	270–276 V	Required to operate the system
Subtract the holder's distance from the target	70 mm	For optimal results
Speed	7–9 rpm	As required
Working pressure	5×10^{-1} Pa	As required
Base pressure	5×10^{-4} Pa	As required
Chiller temperature	20°C	Below 15°C, plasma will not generate.

Abbreviation: PVD, physical vapour deposition.

TABLE 3a | Chemical composition of normal human blood plasma at 7.4 ± 0.1 pH.

Ion	Na^+	Cl^-	Ca^{+2}	Mg^{+2}	K^+	HCO^{-3}	$HPO4^{-2}$	$SO4^{-2}$
Conc. ($mmol^{-1}$)	142.0	103.0	2.5	1.5	5.0	27.0	1.0	0.5

TABLE 3b | Typical composition of artificial saliva 7.4 ± 0.15 pH.

Constituents	KCl (g)	NaCl (g)	$CaCl_2 \cdot 2H_2O$ (g)	$NaH_2PO_4 \cdot 2H_2O$ (g)	$Na_2S \cdot 2H_2O$ (g)	Urea (L)
Amount in 1000 mL	0.400	0.400	0.795	0.780	0.005	1.00

TABLE 3c | Composition of Ringer's solution at 7.4 ± 0.1 pH.

Constituents	NaCl (g)	KCl (g)	$CaCl_2$ (g)	$NaHCO_3$
Amount in 1000 mL	8.64	0.30	0.48	0.200

TABLE 3d | Typical composition of simulated body fluid at 7.4 ± 0.1 pH.

Constituents	NaCl (g)	$NaHCO_3$ (g)	KCl (g)	$(CH_2OH)_3 \cdot C\text{-}NH_3$ (g)	$MgCl_2 \cdot 6\text{-}H_2O$ (g)	1.0 HCl (mL)	Na_2SO_4 (g)	$CaCl_2$ (g)
Amount in 1000 mL	8.035	0.355	0.225	6.118	0.10	39	0.072	0.292

To assess the wear characteristics, a Multi-Function Tribometer (MFT-RTECH INSTRUMENTS) was employed under two different applied loads (5 N and 50 N) with a sliding distance of 10 mm in the human blood environment. Additionally, the topography of the worn surfaces on both the untreated and Ta-coated 316L stainless steel samples was examined using 2D/3D profilometry after the wear tests.

2.6 | Contact Angle Measurement

Contact angle measurements were conducted using the Drop Shape Analyzer-DSA 25 (Kruss) measuring apparatus to determine the wettability of the coatings' surface. The sessile drop technique injects a liquid drop from a syringe into the test material's surface. After the reduction is applied to the material, the advancing CA can

be calculated, often using a goniometer. The progressing angle at the liquid-solid interface is calculated via data analysis after a goniometer records the drop on the specimens.

3 | Results and Discussion

3.1 | Optical Microscopy

The bare and Ta-coated 316L SS microstructure was analysed using an optical microscope. The sample with dimensions $20 \times 20 \times 2$ mm was taken for analysis. Figure 1 shows the optical microscope results of Ta-coated and bare surfaces of 316L Stainless steel. Figure 1b demonstrates a uniform Ta coating, whereas Figure 1a reveals austenitic grains on the bare surface. When examining 316L stainless steel using an optical microscope, the austenitic grains may appear as small, closely packed grains that are difficult to distinguish from one another. The exact appearance and size of the austenitic grains can depend on factors such as the processing history and any subsequent treatments that the material has undergone. The uniformity of the Ta coating over the surface indicates that the coating process effectively produced a consistent and even layer of Ta. Austenitic grains are visible due to their distinct boundaries and shapes, with grain sizes and structures consistent with austenitic stainless steel known for its face-centred cubic (FCC) structure. This structure contributes to the material's excellent toughness and corrosion resistance, making it suitable for biomedical applications. The Ta coating covers the austenitic grains, creating a more uniform surface that masks the original grain structure of the underlying 316L SS. This smooth appearance suggests a dense and possibly amorphous or nanocrystalline Ta layer, which is beneficial for enhancing corrosion resistance and surface hardness.

3.2 | Energy Dispersive Spectroscopy

The energy-dispersive X-ray spectra of 316L stainless steel reveal various peaks related to the components that make up the sample, including Ta, Cr, Mo, manganese (Mn), Ni, and Fe meaning that the passive surface layer is made up of a combination of oxides that represent the elements depicted in Figure 2. The presence of Ta led to give more uniformly homogeneous in Ta-coated surface observed maximum (91.52 wt.%) with other elements like Fe, Cr, Mo, Mn, and Ni (least) after electrochemical corrosion test performed in human blood presented in Figure 2a. It also found the expected peaks of different elements (Cr, Mo, Mn, Ni, and Fe) in different solutions like AS, ringer, and simulated body fluid.

The high-weight presence of Cr and Ni in human blood tested on bare 316L SS indicates that stable oxide layers will be formed in these percentages, where it is known that oxygen causes metal oxides to form in layers. The distribution of primary elements in the substrate is evident for stainless steel-type 316L surfaces. When Cr-oxide formed on the bare surface, the overall amount of Cr was abundantly enriched compared to the bulk concentration (Figure 2b–e). The overall concentration of Fe was substantially lower than in bulk and was the passive layer's second most significant constituent when oxidised elements were considered. Mo-oxide concentration was about the same as it was in bulk.

On the other hand, the Ni element was severely reduced at the topmost layers, and its content rose due to sputtering. The passive layer contained a minimal amount of Mn species compared to the bulk. Therefore, a thorough understanding of the behaviour of oxide films in an in vitro environment is essential to understanding the corrosion phenomenon better because the oxide film that prevents the dissolution of metal ions is not always stable in the human body.

The interactions between the material and the physiological media significantly impact how quickly the oxide layer reforms and how long it takes to do so. Re-passivating, also known as regeneration, requires variable amounts of time depending on the material used. The regeneration period mentioned earlier affects both the rate of corrosion that occurs after a disruption and the amount of metal ions released. Literature survey data conclude that the regeneration time in Ti–6Al–4V is shorter and longer in stainless steel. Compared to traditional alloys like Co–Cr and Ti–6Al–4V, the surface oxide layer stability of 316L stainless steel and Ni–Ti is not exceptionally high, and there is a higher probability that metal ions will be released. Because it will slow down corrosion, a coating provided to the implants is highly preferable [31, 32].

3.3 | SEM

Figure 3 presents SEM images that reveal no observable changes on the Ta-coated 316L stainless steel surface after undergoing

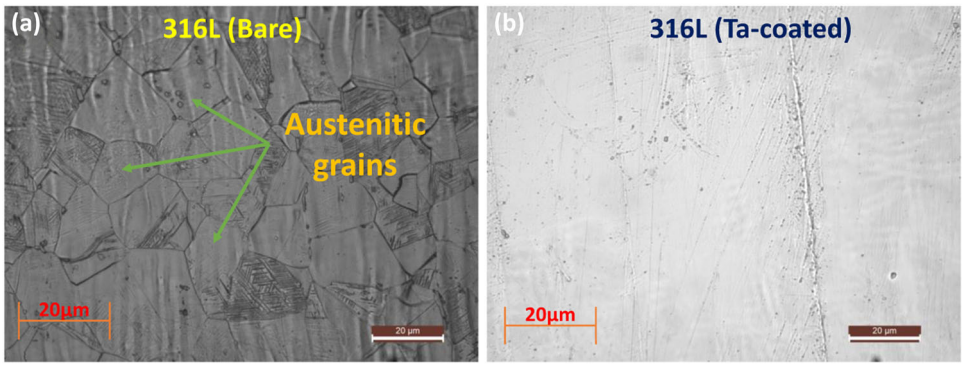

FIGURE 1 | Optical microscopy images of 316L stainless steel (a) Bare surface. (b) Ta-coated surface. [Color figure can be viewed at wileyonlinelibrary.com]

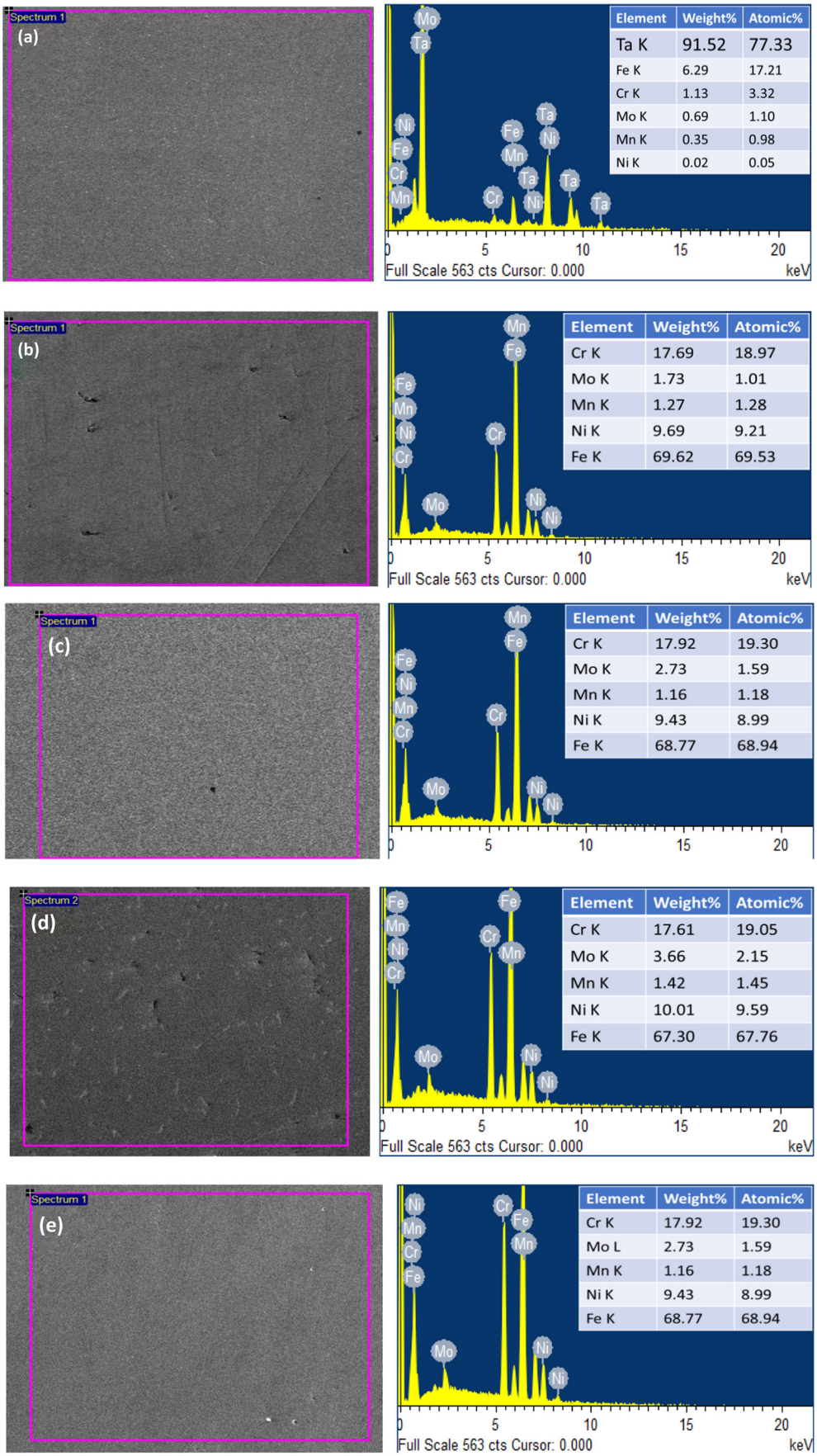

FIGURE 2 | Elemental diffraction X-ray spectroscopy images 316L SS in different solutions at 100 μm (a) Ta-coated in human blood, (b) bare in human blood, (c) bare in artificial saliva, (d) bare in ringer, and (e) bare in simulated body fluid (SBF). [Color figure can be viewed at wileyonlinelibrary.com]

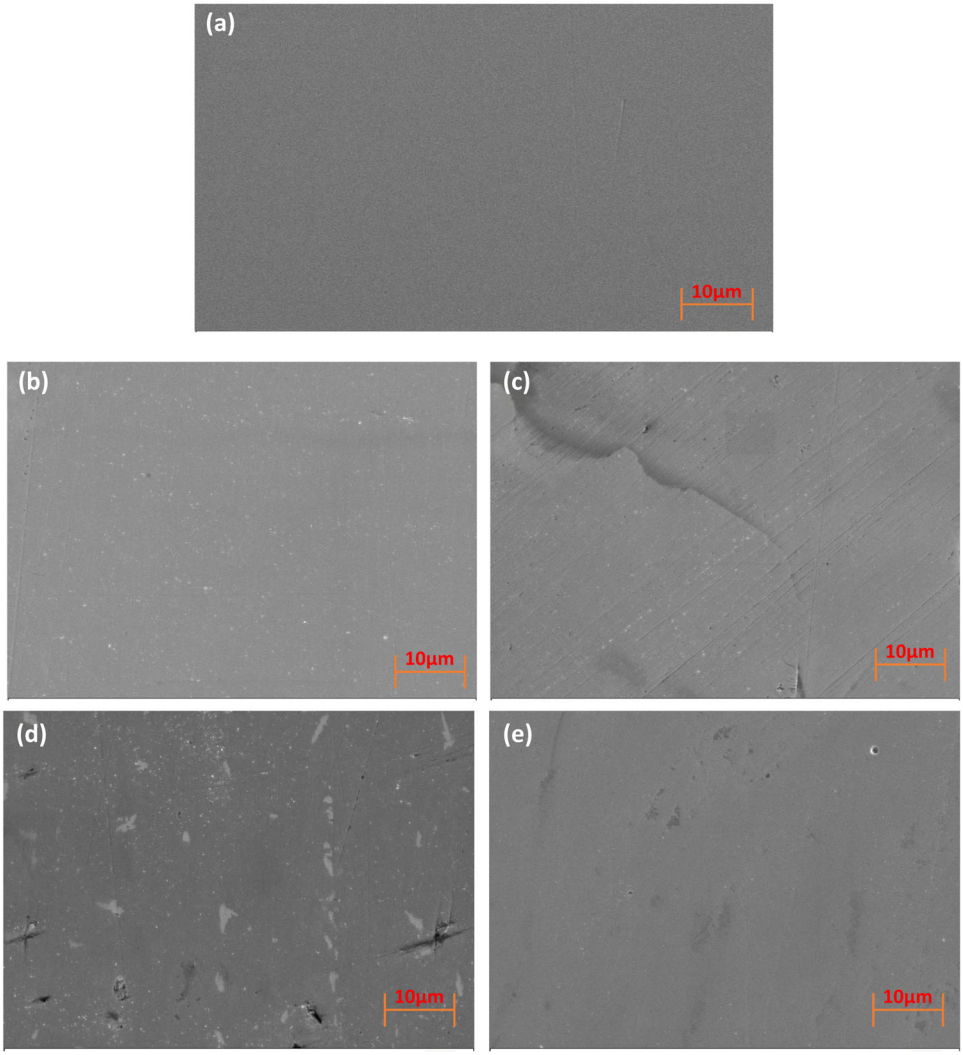

FIGURE 3 | Scanning electron microscopy images 316L SS in different solutions (a) tantalum (Ta)-coated in human blood, (b) bare in human blood, (c) bare in artificial saliva, (d) bare in ringer, and (e) bare in simulated body fluid (SBF). [Color figure can be viewed at wileyonlinelibrary.com]

electrochemical corrosion testing in a simulated human blood environment. The absence of pits and any disruptions in the surface morphology, as shown in Figure 3a, indicates the material's resistance to corrosion in such conditions. Therefore, this modified stainless steel (316L) can be employed as an implant in biomedical applications where a fluid medium is human blood. Figure 3b also has nearly the same observations, that there are no changes on the sample's surface, which means this sample is of 316L SS. In Figure 3c, it is visible that there are many scratches on the surface of the sample, which means this sample of 316L SS is eroded in the Ringer solution. Therefore, this steel sample cannot be employed as an implant in biomedical applications where a fluid medium is a Ringer solution. In Figure 3d, it is visible that there are no changes on the surface of the sample, which means this sample of 316L SS is not corroded in SBF. Therefore, this steel sample can be employed as an implant in biomedical applications where a fluid medium is SBF. As seen in Figure 3d, the specimens were covered with brittle, dense, lumpy deposits of black corrosion products, ultimately allowing the surface cracks to be seen. The SEM micrographs of corrosion pits for stainless steel surfaces reveal nearly no localised corrosion on the metal surface after exposure to the ringer solution. Referring to the previous studies [29, 30], This is where the microstructure of the Ta film that was deposited on Ta on SS can be observed; the size of the Ta layer formed on the surface of the steel is around 50 nm.

The paragraph describes the cross-sectional SEM morphology and element distribution in depth of Ta coatings. The coatings were deposited for 15 min, and the resulting cross-sections were dense with no visible cracks or holes at the coating or coating/substrate interfaces. The major element in the coating was found to be Ta, as observed from EDS images. A diffusion layer was observed at all coating/substrate interfaces, and its thickness in the Ta coatings deposited for 15 min was found to be in the range of 2–2.5 μm. This thickness was higher than that observed in Ta coatings deposited by the CVD method, which was found to be 1 μm [33]. The accumulation of target atoms on the substrate surface and the interdiffusion of elements at the coating/substrate interface were also recognised as the main processes involved in the coating.

The surface topography of materials can play a significant role in their biological performance. In the case of Ta coatings, the surface topography can influence the coating's ability to integrate with bone tissue, which is critical for its long-term stability in the body.

Research has shown that micro and nanostructured surfaces can enhance the biological properties of biomaterials [34]. The micro and nano-sized features can mimic the morphology of natural bone, which can promote cellular adhesion, proliferation, and differentiation. Moreover, the micro and nanostructured surfaces can increase the surface area, facilitating better protein adsorption and subsequent cell adhesion. Therefore, by modifying the surface topography of Ta coatings to include micro and nanostructures or micro/nano-textured structures, we can improve their physical performance, leading to better integration with bone tissue and long-term stability in the body [35–37].

3.4 | XRD

The Ta coating deposited at 15 min. times is depicted in Figure 4 as XRD patterns. The peaks (03) corresponding to face-centred cubic (FCC) austenitic stainless steel, β-Ta, Ni_2-Ta, and Fe_2-Ta phase peaks can also be seen in the Ta coating pattern deposited for 15 min. Whereas the Ta2C, Fe Ta, and Fe2Ta phases are supposed to be residues of the interfacial diffusion reaction between the Ta coatings and 316L SS, the phase β-Ta mainly originated from the sputter-deposited Ta coatings in Figure 4b. The variations in Ta intensity show that Ta coatings deposited for short periods (15 min) primarily constitute β-Ta. In comparison, those deposited for extended periods exceeding 30 min are mainly made of α-Ta [12]. Also, the interfacial phases should have more content with longer diffusion-reaction times, but instead, they gradually disappear, most likely because the higher Ta coating thickness lowers their peak intensities [26].

The diffractogram of the Ta-coated 316L stainless steel substrate is represented in Figure 4b, which displays a mixture of Ni and tantalum (Ni_2-Ta) at 31.914°, 33.4822°, and 37.6234° [ICSD-98-010-2816], Cr–Ni at 41.2355 (ICSD-98-010-2819), pure Ta (ICSD-98-065-2900) and β-Ta phase pick positions at 33.4822° and 37.6234° (ICSD-98-005-4207). The grazing angle XRD of the Ta layer was created on a single layer of Ta/SS. The (002), (211), and (213) reflections of Ta, as well as those corresponding to the nanocrystalline β-Ta phase and Ta, as well as the austenitic phase of the steel substrate, are shown in the diffractogram. The Ta reflections were obtained with lower-intensity Ta deposition on steel, offering a substantial coating. The Cr–Ni and Cr–Fe compounds were found in bare 316L stainless steel, shown in Figure 4a.

3.5 | Contact Angle Measurement

The bare and Ta-coated 316L SS contact angle was examined using a goniometer at a relative humidity and temperature of 35% and 32°C ± 1, respectively. Deionised drop mode at a rate of 2.66 L/s, Volume 2, was used for the investigations. Images of the droplet shape on the machined workpiece were taken at intervals of 5 s using a super-speed digital camera (U4 series, 520 frames per second) and ellipse (Tangent-1) fitting method. A pipette was used to ensure that each time a drop of deionised distilled water (about 2 L) was applied to the sample, it was performed according to the method illustrated in Figure 5. Four measurements were taken for each surface treatment. The average static contact angle was calculated. The Ta films' wettability and surface energy were evaluated using sessile contact angle techniques. Both the coated and non-coated surfaces were observed as hydrophilic, as depicted in Figure 5. The Ta-coated 316L stainless steel was found to be more hydrophilic than the bare, indicating the cell adhesion proximity will be more in the coated surface.

4 | Electrochemical Corrosion Analysis

4.1 | OCP

Based on the OCP's results, the samples pretend to be stable. The primary objective of OCP's results is to offer information on the status of the material's surface; with the help of the results obtained, it can be determined whether the material is active or passive. The OCP monitoring of 316L stainless steel immersion

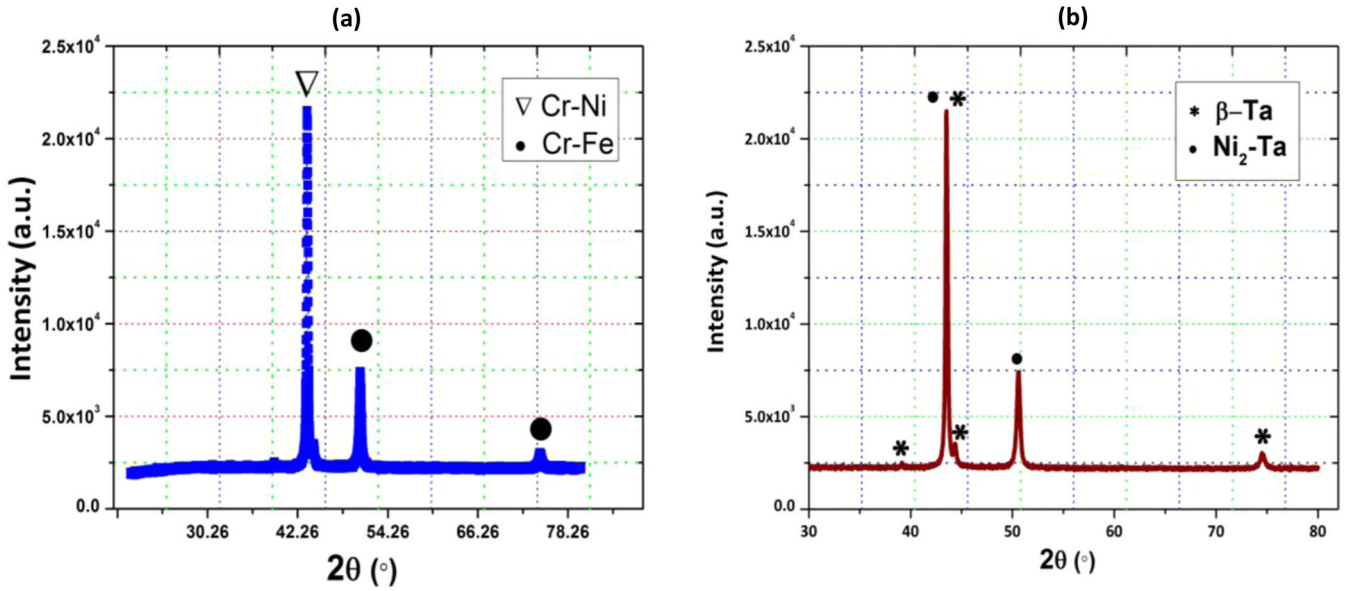

FIGURE 4 | X-ray diffraction results of 316L stainless steel (a) bare (b) tantalum (Ta)-coated. [Color figure can be viewed at wileyonlinelibrary.com]

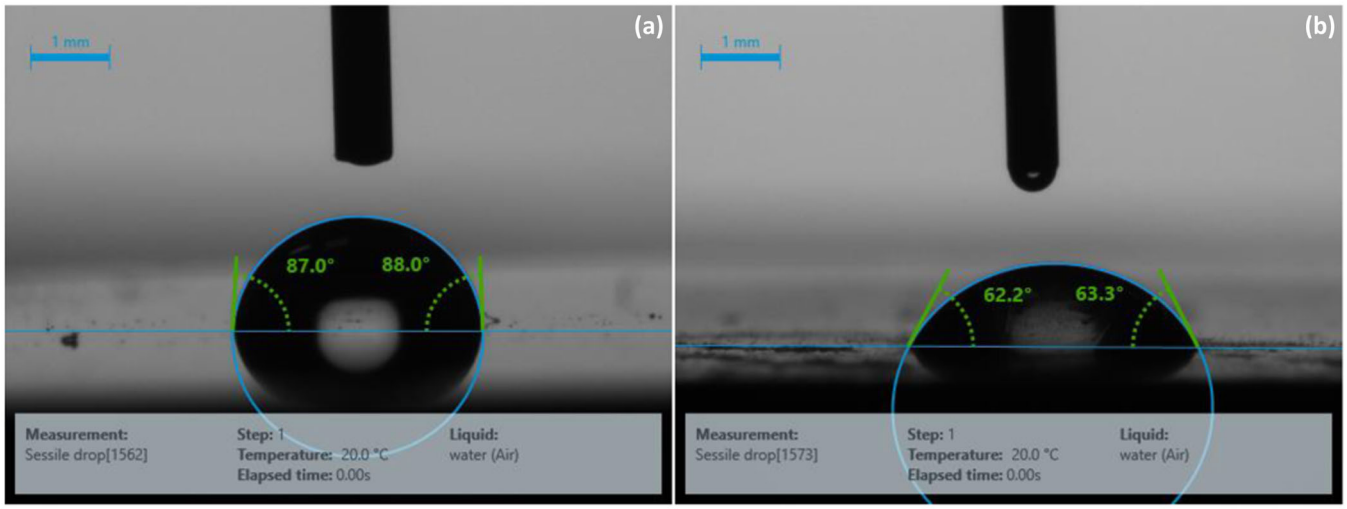

FIGURE 5 | Contact angle measurement result of 316L SS (a) bare (b) tantalum (Ta)-coated. [Color figure can be viewed at wileyonlinelibrary.com]

in human blood, saliva solution, simulated body fluid, and Ringer solution was performed for 30 min each at room temperature.

Figure 6 shows that OCP runs from high potential to low potential, which means that the immersed sample of 316L stainless steel is in a passive state, further suggesting that this sample is corrosion-resistant (Figure 6a). Therefore, this steel sample can be additionally employed as an implant in biomedical applications where a fluid medium is human blood. In Figure 6b, it is visible that OCP runs from low potential to high potential, which means that the immersed sample of 316L stainless steel is in an active state, which further suggests that this sample is not much corrosion-resistant. In Figure 6c, it is visible that OCP runs from high potential to low potential, which means that the immersed sample of 316L stainless steel is in a passive state, which further means that this sample is corrosion-resistant. In Figure 6d,e, it is visible that OCP runs from low potential to high potential, which means that the immersed sample of 316L stainless steel is in an active state, which reveals the stability with respect to time. And, bare 316L stainless steel sample observed less stability in SBF compared to HB.

4.2 | EIS

The study investigated the corrosion behaviour of a porous oxide layer and the effect of adding a Ta layer on its corrosion resistance. The addition of a Ta layer may result in the production of a much more protective corrosion product. However, increasing Ta content may lead to the corrosion product's protection capacity degradation, indicated by the slight decrease in the R1 value. To quantitatively analyse the corrosion resistance, the total resistance (Rt) of bare and coated 316L SS is calculated as 0.0029 and 0.003, respectively. The highest Rt is for Ta-coated 316L stainless steel. The Rt is calculated as the sum of the Warburg impedance (Rw), the charge transfer resistance (R2), and (R1), with the solution resistance (Rs) omitted because it is essentially constant. The comparative analysis of the Rt value suggests that the modification in 316L SS can improve its corrosion resistance. The polarisation and EIS test results support this conclusion. In summary, adding a Ta layer enhances the corrosion resistance of 316L SS, and the Rt is used to analyze its corrosion resistance quantitatively.

A summary of the associated electrochemical parameters with the corresponding electric circuit for evaluating EIS spectra is shown in Figure 7. Also, the high Epit values of all the Ta coatings nearly two orders of magnitude greater than those of the original 316L SS—indicate improved resistance to pitting corrosion. Table 4 shows that Ta coatings deposited during 15 min have a more significant E_{corr} than those of the 316L SS substrate and a lower passive current. Still, the 316L SS for SBF has a lower E_{corr}. This shows that 316L stainless steel without a coating is more susceptible to corrosion.

In contrast, Ta coating can increase the corrosion resistance of 316L SS in human blood and strengthen electrochemical activity. Electrochemical tests were carried out to investigate the corrosion resistance of Ta-coated 316L SS in different solutions. Figure 8 demonstrates the Nyquist plots of 316L in various mediums.

The EIS test was carried out at room temperature by sweeping the range from 0 to 1.2×10^5 Hz at a 10 mV/min scan rate in different fluid media. To determine the relative stability of the protective film generated on the surface of 316L stainless steel, impedance spectra were acquired at passive potential during the creation of the passive film. Rs, constant phase element (CPE), resistance of porous product layer of corrosion (R1), resistance of alloy interface and product of corrosion (R2), and Rw are the components of the equivalent electric circuit demonstrated in Figure 7. The fitting parameter acquired from EIS data that is well-fitting in the EEC model is shown in Table 4. The data obtained after fitting are evaluated using a standard deviation (x^2) and a magnitude of around 10^4. As a result, we may presume that the EEC models offered are suitable for evaluating the electrochemical interface's behaviour experimentally. The electrochemical impedance parameters were calculated using the pitting approach.

EIS characterisation is essential for the analysis of materials. Data about the interface, design, and responses can be found in

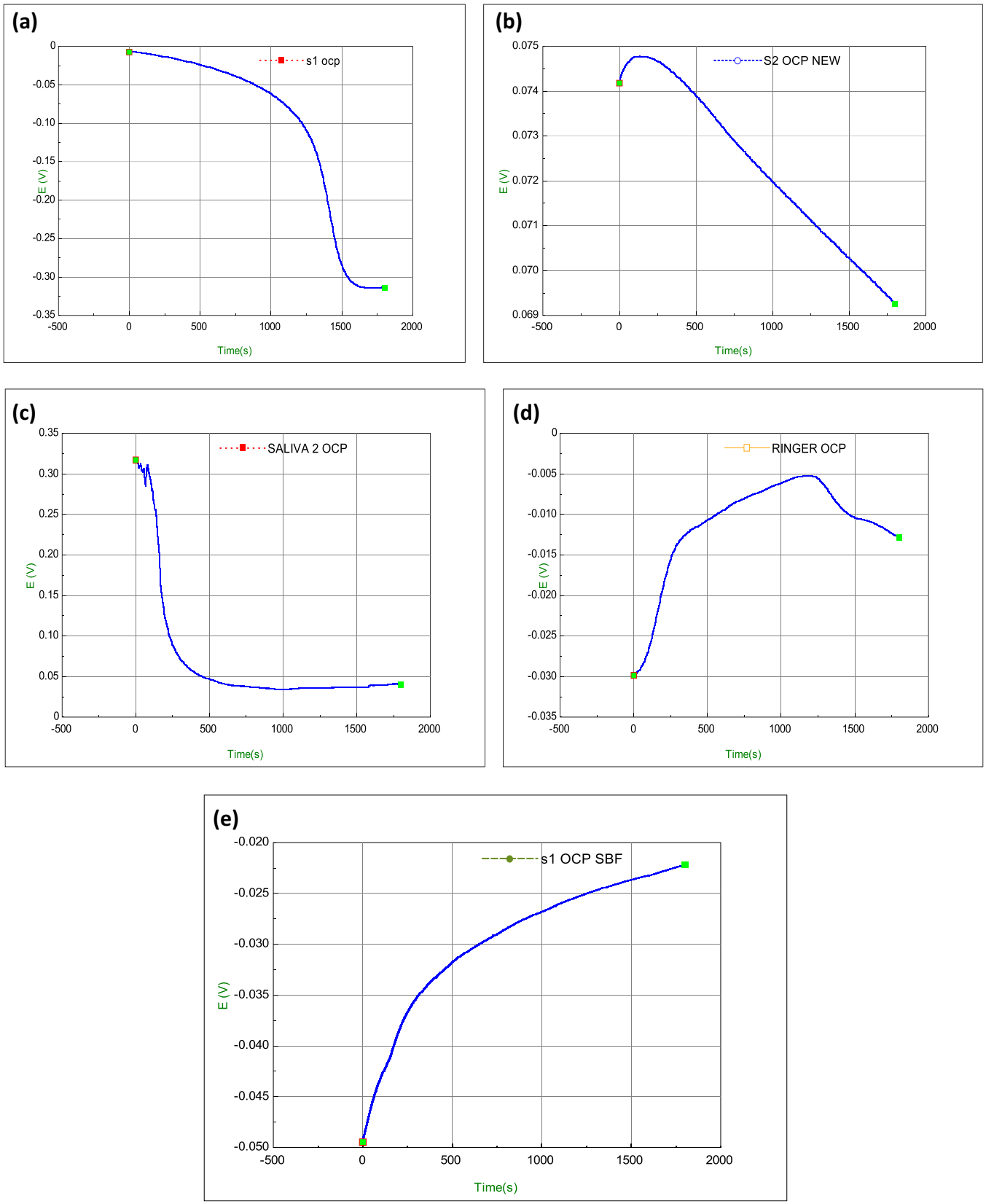

FIGURE 6 | Open circuit potential plot of 316L SS in different solutions (a) Ta-coated in human blood, (b) bare in human blood, (c) bare in artificial saliva, (d) bare in Ringer, and (e) bare in simulated body fluid (SBF). [Color figure can be viewed at wileyonlinelibrary.com]

the system response analysis. The data obtained is in the form of the base diagrams showing the modulus of impedance |Z (m)| and the phase angle against the logarithm of the frequency [38] as well as the Nyquist graphs, which display the imaginary part of the impedance (Z″) against the real part (Z′) [39]. The capacitive behaviour of the various substrates is shown by the slopes determined from the Nyquist diagrams in the following order: It includes etched stainless steel (etched SS), Ta-coated stainless steel (Ta/SS), and Ta layer-coated stainless steel. High frequencies result in a drop-in log Z, which exhibits a distinctive and capacitive behaviour in the low to medium frequency range [39].

Additionally, compared to the coated material, this substrate exhibits a greater Log Z versus frequency in the linear range and phase angle plateau. The coating's isolating effect is attributed to this result [40]. Due to the observed delamination, the Ta film on SS would not function as a reliable protective coating. A-Ta film placed on SS316LVM exhibits delamination because of the extremely high strain at the interface [31, 32].

It is observed from Table 4 that when SS 316L was immersed in Human Blood, the total resistance was 138,573.2 Ωcm^2. Then SS 316L was immersed in SBF, and the total resistance was decreased from 138,573.2 Ωcm^2 to 1862.862 Ωcm^2. When SS 316L was immersed in Ringer solution, total resistance was reduced from 1862.862 Ωcm^2 to 1749.33 Ωcm^2. When SS 316L was immersed in Saliva, total resistance was decreased from 1749.33 Ωcm^2 to −3746.5287 $\Omega cm^{2.}$ From these data, it can be concluded that SS 316L was more corrosion-resistant in human blood than SBF, Ringer, and saliva.

Figure 8a represents the Nyquist plot of 316L SS in human blood in which real impedance (Zre) is taken as 95,000 k Ωcm^2, and imaginary impedance (Zim) is taken as 7×10^4 k Ωcm^2. Figure 8b represents the Nyquist plot of 316L SS in Ringer solution in which Zre is taken as 2.25×10^5 k Ωcm^2 and Zim is taken as 5.8×10^4 k Ωcm^2. Figure 8c represents a Nyquist plot of 316L SS in Saliva in which Zre is taken as 1,180,000 k Ωcm^2, and Zim is taken as 1.6×10^5 k Ωcm^2. Figure 8d represents the Nyquist plot of 316L SS in SBF in which Zre is taken as 225,000 k Ωcm^2 and Zim is taken as 4.9×10^5 k Ωcm^2.

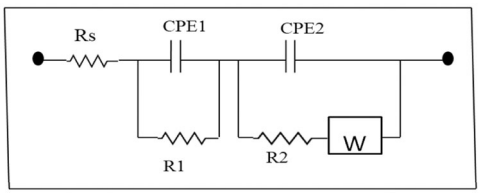

FIGURE 7 | Equivalent electric circuit for analysis of electrochemical impedance spectroscopy (EIS) spectra. CPE, constant phase element; R1, resistance of porous product layer of corrosion; R2, resistance of alloy interface and product of corrosion; Rs, solution resistance; W, Warburg impedance.

4.3 | Potentiodynamic Polarisation (PDP)

The PDP curves of 316L stainless steel in human blood, Ringer solution, saliva, and SBF are shown in Figure 9. Table 5 lists the corrosion parameters, which include E_{corr}, Tafel slopes (β_c = cathodic, β_a = anodic), CR, and corrosion current (I_{corr}). The experiment involved measuring each sample's I_{corr} density by extrapolating the cathodic and anodic branches of the polarisation curves. The results showed that the E_{corr} of the coated samples was nobler than that of the bare 316L SS substrates. This is because the metallic nature of the Ta-coated surface protected the substrate surface from corrosion.

It is observed from Table 5 that the 316L SS (Ta-coated) was immersed in human blood, the I_{corr} was 1.2445E-07 A/cm^2, and the CR was 0.146×10^{-2} mm/a, and the 316L SS (bare) was immersed in human blood the I_{corr} was 2.7410E-09 A/cm^2, and the CR was 0.325×10^{-2} mm/a. Then SS 316L was immersed in Saliva, the I_{corr} was 4.7452E-07 A/cm^2, and the CR was 0.556×10^{-2} mm/a. When SS 316L was immersed in Ringer solution, the I_{corr} was 6.6486E-07 A/cm^2, and the CR was 0.779×10^{-2} mm/a. When SS 316L was immersed in SBF, the I_{corr} was 1.2148E-06, and the CR was increased by 1.425 mm/a. These data concluded SS 316L was more corrosion-resistant in human blood than saliva, ringer, and SBF.

Based on the PDP results, the study compared the electrochemical behaviour of coated and uncoated 316L SS in different solutions. The study measured the potential polarisation curve and monitored the formation of the passive layer and corrosion products during the experiment. The I_{corr} density was determined by extrapolating the cathodic Tafel area, a method used to analyse the corrosion kinetics of the alloy. Icorr is the alloy CR at the E_{corr} depicted in Figure 9. The E_{corr} was found to shift from negative 1.2148E-06 mV to a more negative value, indicating a negative shift trend. A nobler value of E_{corr} suggests that the alloy is harder against corrosion, and thus, the Ta

TABLE 4 | Parameters of the equivalent electrical circuit (EEC) model 316L SS samples in different mediums.

Solutions (Ta-coated and bare 316L)	R_s Ωcm^2	R_1 Ωcm^2	CPE_1 $Y_1 \times 10^{-6}$ $\Omega cm^{-2}s^n$	CPE_1 n_1	R_2 Ωcm^2	CPE_2 $Y_2 \times 10^{-9}$ $\Omega cm^{-2}s^n$	CPE_2 n_2	R_w Ωcm^2	$\chi^2 \times 10^{-4}$
Human blood	240.1	96880	0.000105	0.8897	0.10081	0.00011	0.983	41453	0.0029
Saliva	544.3	1.45	3.71	0.277	0.0213	9.3249	1.167	1695	0.003
Ringer	53.11	1.26	3.31	0.8350	0.0213	9.3249	1.167	1695	0.003
SBF	53.16	1.10	7.49	0.6996	1060	1.0097	1.000	748.6	0.003

Abbreviations: CPE, constant phase element; R_1, resistance of porous product layer of corrosion; R_2, resistance of alloy interface and product of corrosion; R_s, solution resistance; R_w, Warburg impedance; Ta, tantalum.

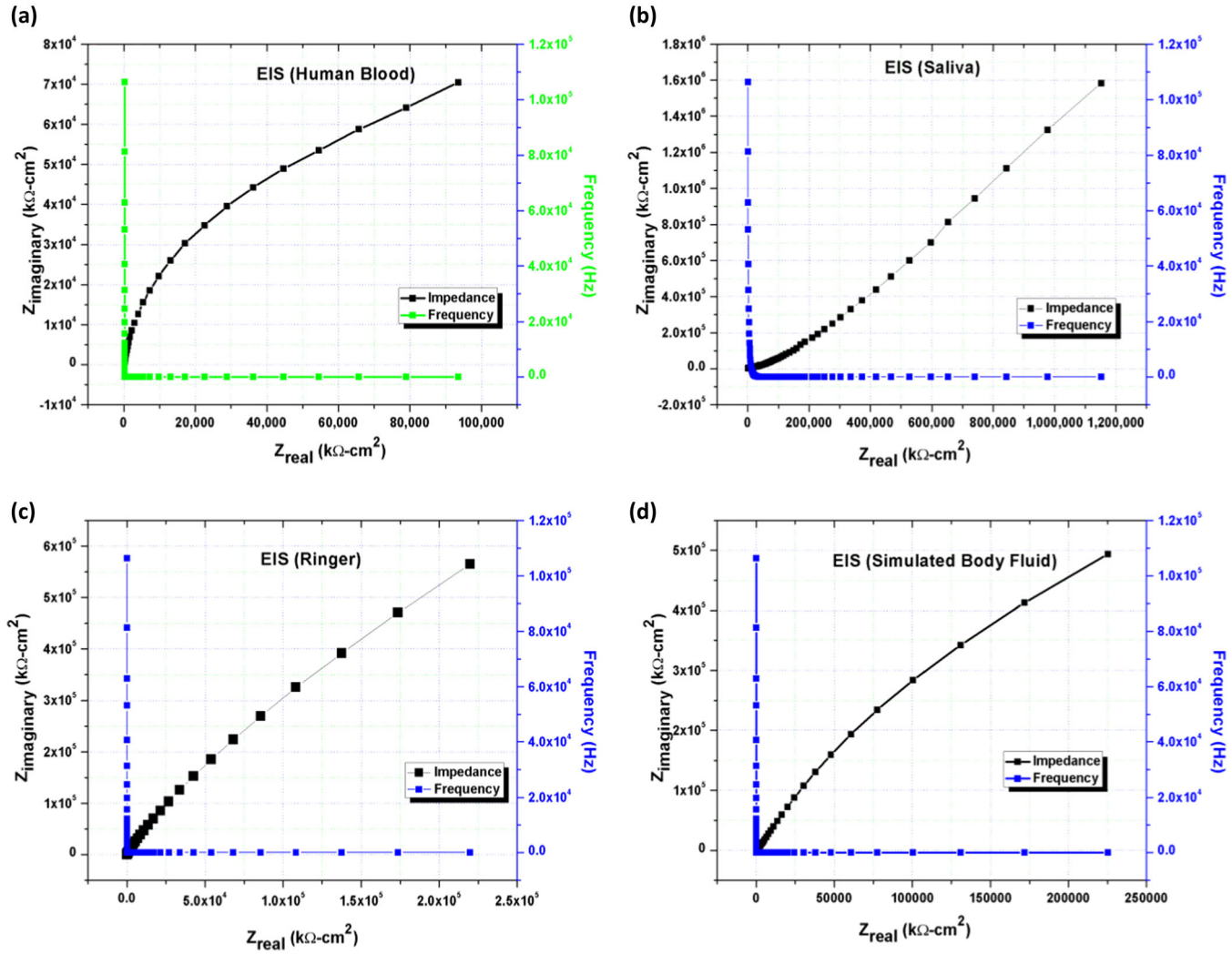

FIGURE 8 | Nyquist plots of 316L in different mediums, (a) human blood, (b) Ringer, (c) saliva, (d) simulated body fluid (SBF). [Color figure can be viewed at wileyonlinelibrary.com]

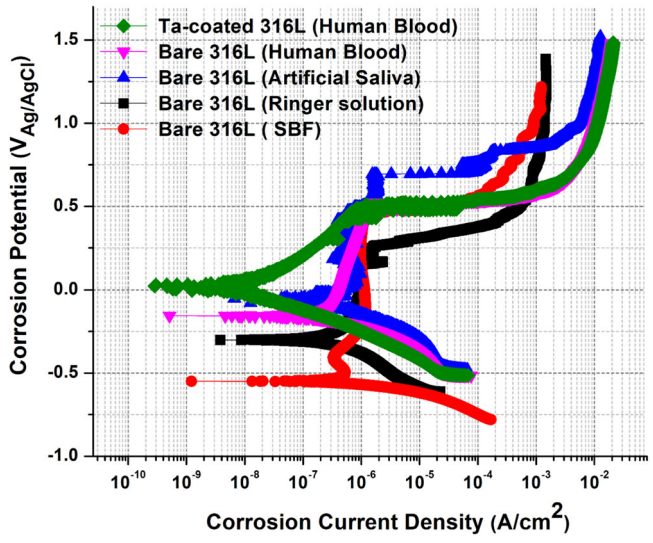

FIGURE 9 | Potentiodynamic polarisation curve of Ta-coated and bare 316L SS in different solutions. SBF, simulated body fluid; Ta, tantalum. [Color figure can be viewed at wileyonlinelibrary.com]

coating is quickly found to improve its corrosion resistance. In summary, the study found that the Ta coating improved the corrosion resistance in the human blood environment of 316L SS, and Icorr was used as a metric to analyse the corrosion kinetics of the substance.

316L SS exhibits the highest corrosion resistance in human blood, followed by saliva, Ringer solution, and SBF. Notably, these conclusions were drawn based on polarisation studies commonly used to investigate the corrosion behaviour of metallic materials. However, other factors such as temperature, flow rate, and solution composition can also affect the corrosion behaviour of SS 316L in different environments. Therefore, further studies (in vivo) may be needed to validate and understand the corrosion behaviour of Ta-coated 316L stainless steel before clinical trials. The CR and I_{corr} are increasing from Human Blood to SBF.

Based on the results of the polarisation studies, it can be concluded that the corrosion behaviour of SS 316L varies depending on the environment it is exposed to. The values of the CR and I_{corr} increase from human blood to SBF, indicating a higher tendency for corrosion in the latter. Furthermore, the order of

TABLE 5 | Potential polarisation results of bare and Ta-coated 316L in different solutions.

Solutions	E_{corr} (Volts)	β_a (mV)	β_c (mV)	I_{corr} (A/cm^2)	CR × 10^{-2} (mm/a)
Human blood (Ta-coated 316L)	0.0631	224.11	105.41	1.2445E-07	0.146
Human blood (316L SS)	0.0147	112.36	90.795	2.741E-09	0.325
Saliva	0.5494	2282.90	65.268	4.7452E-07	0.556
Ringer	0.1557	1315.74	162.92	6.6486E-07	0.779
SBF	0.3002	3767.65	331.50	1.2148E-06	1.425

Abbreviations: β_a, Tafel slopes anodic; β_c, Tafel slopes cathodic; CR, corrosion rate; E_{corr}, corrosion potential; I_{corr}, corrosion current; Ta, tantalum.

corrosion resistance of SS 316L in different environments can be listed as follows:

Human blood > Artificial saliva > Ringer solution > Simulated body fluid.

5 | Wear Behaviour of Ta-Coated 316L SS in Human Blood

The samples' wear characteristics were evaluated using a multifunctional tribometer in an environment similar to human blood under specific stresses and a constant temperature of 37°C. The sample's weight was measured on a digital balance (Model No. K-BA 200) both before and after testing to assess the amount of weight loss. For both bare and Ta-coated 316L Stainless Steel samples, the weight loss and coefficient of friction (COF) were noted. Archard's equations are used to determine volume loss and wear rates. These equations consider several aspects, including material hardness, sliding distance, applied stress, and measured weight loss. The volume loss and wear rates of both bare and Ta-coated 316L SS samples were calculated using these formulas and information derived from weight loss measurements and COF values.

During the investigation into the wear behaviour of the samples, it also analysed the COF changes over time, which provides insights into the evolving wear patterns on the samples as a function of time, enabling us to conclude surface roughness or smoothness based on our findings. As such, Figure 10 depicts the relationship between the friction coefficient and time for two applied loads, 5 N and 50 N.

A coating's vulnerability to failure from elastic strain is commonly assessed through the H/E ratio. Likewise, the resistance of a coating to fracture resulting from plastic deformation, including elastoplastic deformation, is associated with its fracture toughness, expressed as the ratio H3/E2 [17]. Consequently, a higher H/E ratio indicates superior wear resistance for a specific coating. Notably, the H/E ratio for stainless steel is approximately 0.015, whereas the coating has an H/E ratio of about 0.026 [41].

Table 6 provides data on the wear characteristics of the samples (316L Stainless Steel and Ta-coated 316L Stainless Steel) under varying loads of 5 N and 50 N. The wear test result shows the wear rate found to be maximum (0.25 $[mm^3/Nm] \times 10^{-5}$) for the bare 316L stainless steel, while the minimum wear rate (0.086 $[mm^3/Nm] \times 10^{-5}$) found in Ta-coated 316L Stainless steel.

The COF is a valuable indicator of a specimen's wear resistance during the wear process. Typically, a lower COF signifies more excellent wear resistance. To assess the wear performance of Ta-coated 316L SS under typical operating conditions, wear resistance tests were conducted at normal speeds, with 316L SS serving as a comparative reference. During low-speed wear, the COF of the 316 substrates steadily increased over time, whereas the COF of the coated surface gradually reached a stable level. In particular, the Ta-coated 316L SS displayed a progressive improvement in wear resistance along the build direction at low-speed friction, characterised by the lowest average COF and wear track depth on the surface. This enhancement in wear resistance was especially evident in scenarios involving oxidation wear and adhesive wear at high-speed friction, distinguishing it from the performance of 316L [42]. A 1.08 μm thick coating of ZrCxN1−x was applied to AISI 316L, and the impact of deposition temperature on phase composition, mechanical characteristics, corrosion resistance, and blood compatibility results show the mechanical testing obtained that the nanohardness and elasticity modulus of the ZrCxN1−x coatings achieved their highest values, coinciding with the formation of nanocrystalline Zr_2CN. Electrochemical assessments indicated a significant enhancement in the corrosion resistance of AISI 316L due to the presence of the ZrCxN1−x coating, with the one deposited at 400°C exhibiting the best performance [43].

Figure 11 shows that the wear surface is notably more pronounced than other topographical images Figure 11a, indicating that bare 316L is susceptible to more significant wear when subjected to higher loads. Conversely, in Figure 11b, we observe a more consistent wear pattern on the sample's surface after applying a Ta coating. In Figure 11c, irregularities are evident on the wear surface, which is nonuniform. The wear surface in all images is less prominent than in Figure 11a. Similarly, in Figure 11d, the wear surface is less pronounced but somewhat broader compared to bare 316L SS due to the presence of the Ta coating.

In each instance of surface modification, Ra and Rp values were consistently elevated compared to untreated steel. The study examined surface characteristics, encompassing roughness (Ra and Rp) and wettability (CA), for bare steel and various polymer and polymer-peptide coatings. The findings demonstrated an evident interdependence among surface chemistry, roughness, and wettability, collectively influencing cell adhesion. Notably,

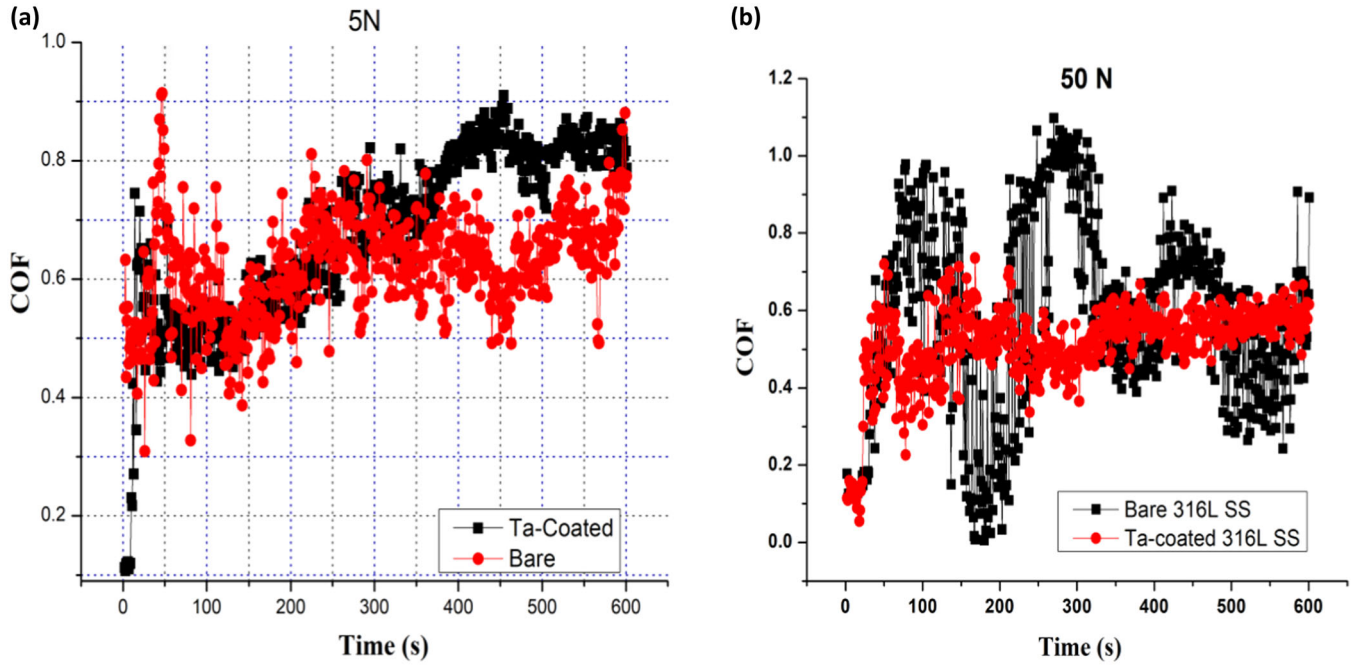

FIGURE 10 | Coefficient of Friction versus time images of bare and tantalum (Ta)-coated 316L SS (a) at 5 N (b) at 50 N. [Color figure can be viewed at wileyonlinelibrary.com]

TABLE 6 | Wear test results of bare and tantalum (Ta)-coated 316L stainless steel.

Material (316L SS)	Load (N)	Mass before test (g)	Mass after test (g)	Mass loss (g)	Density (g/cm^3)	Volume loss (mm^3)	Sliding distance (mm)	Wear rate (mm^3/Nm) × 10^{-5}
Bare	5	6.0945	6.0943	0.0002	8	0.00014	10	0.28
	50	6.0943	6.0934	0.0009	8	0.0001125	10	0.224
Ta coated	5	7.0714	7.0712	0.0002	16	0.0000562	10	0.112
	50	7.0712	7.0705	0.0007	16	0.0000438	10	0.086

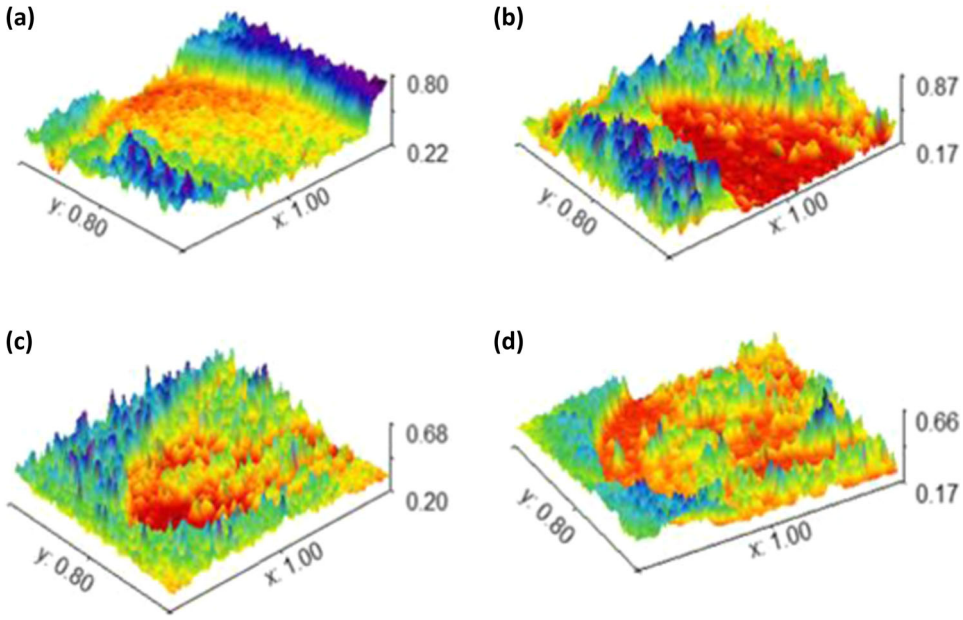

FIGURE 11 | Three-dimensional topographical images of 316L SS (a, b) Bare surface at 5 N and 50 N, (c, d) tantalum (Ta)-coated surface at 5 N and 50 N. [Color figure can be viewed at wileyonlinelibrary.com]

wettability emerged as the predominant factor influencing this synergy [44].

6 | Conclusions

OCP measurements indicated that the Ta-coated 316L SS maintained a passive state across the various testing fluids, with OCP shifting from higher to lower potential values within this stable passive range. EIS exhibits the highest corrosion resistance in human blood compared to other fluids. It suggests that while blood is corrosive, it still allows Ta-coated 316L SS to perform more reliably than in other fluids due to the coating's stabilising effect. PDP results showed a progressive increase in CR and I_{corr} from human blood to ringer, saliva and simulated body fluid ($0.146–14.25 \times 10^{-2}$ mm/a), respectively. The Ta coating enhances the material's electrochemical stability and prevents surface degradation, making it an excellent candidate for biomedical implants exposed to blood. The promising performance in corrosion tests suggests that Ta-coated 316L SS could minimise risks associated with implant corrosion, thus potentially extending implant lifespan and improving performance in high-chloride, protein-rich environments common in the human body. The wear test results show that the wear rate for bare 316L stainless steel is maximum (0.25 [mm^3/Nm] 10^{-5}), while Ta-coated 316L stainless steel has a minimum wear rate of (0.086 [mm^3/Nm] 10^{-5}). The study found that Ta-coated 316L stainless steel performed better in human blood than bare 316L stainless steel, making it a potentially useful material for orthopaedic implant applications.

Acknowledgements

Funding for the project was granted by India's Science and Engineering Research Board (SERB) under Project No. R&D/SERB/MET/19-20/04. The research and experimental resources were provided by the "Indian Institute of Technology Banaras Hindu University" (IIT-BHU), Varanasi, 221005, India, for which the authors are grateful.

Conflicts of Interest

The authors declare no conflicts of interest.

Data Availability Statement

The data that support the findings of this study are available from the corresponding author upon reasonable request.

References

1. D. D. Kumar and G. S. Kaliaraj, "Multifunctional Zirconium Nitride/Copper Multilayer Coatings on Medical Grade 316L SS and Titanium Substrates for Biomedical Applications," *Journal of the Mechanical Behavior of Biomedical Materials* 77 (2018): 106–115, https://doi.org/10.1016/j.jmbbm.2017.09.007.

2. R. J. Lu, X. Wang, H. X. He, et al., "Tantalum-Incorporated Hydroxyapatite Coating on Titanium Implants: Its Mechanical and in Vitro Osteogenic Properties," *Journal of Materials Science: Materials in Medicine* 30, no. 10 (2019): 111, https://doi.org/10.1007/s10856-019-6308-9.

3. L. Geyao, D. Yang, C. Wanglin, and W. Chengyong, "Development and Application of Physical Vapor Deposited Coatings for Medical Devices: A Review," *Procedia CIRP* 89 (2020): 250–262, https://doi.org/10.1016/j.procir.2020.05.149.

4. N. Eliaz, "Corrosion of Metallic Biomaterials: A Review," *Materials* 12, no. 3 (2019): 407, https://doi.org/10.3390/ma12030407.

5. T. Li, P. C. Zhang, K. Liu, et al., "Performance of Tantalum Modified 316L Stainless Steel Bipolar Plate for Proton Exchange Membrane Fuel Cell," *Fuel Cells* 19, no. 6 (2019): 724–730, https://doi.org/10.1002/fuce.201900099.

6. P. Guzmán, W. Aperador, and L. Yate, "Enhancement of the Pitting Corrosion Resistance of AISI 316LVM Steel With Ta-Hf-C/Au Bilayers for Biomedical Applications," *Journal of Nanomaterials* 2017 (2017): 1–10, https://doi.org/10.1155/2017/6825250.

7. G. Manivasagam, D. Dhinasekaran, and A. Rajamanickam, Biomedical Implants: Corrosion and Its Prevention-A Review," *Recent Patents on Corrosion Science* 2 (2010): 40–54.

8. R. A. Antunes and M. C. Lopes De Oliveira, "Corrosion Processes of Physical Vapor Deposition-Coated Metallic Implants," *Critical Reviews in Biomedical Engineering* 37 (2009): 425–460.

9. M. Fathi, M. H. Fathi, and V. Mortazavi, "Tantalum, Niobium and Titanium Coatings for Biocompatibility Improvement of Dental Implants Bioceramics View project Two-Step Sintering of Fluoridated Hydroxyapatite View project Tantalum, Niobium and Titanium Coatings for Biocompatibility Improvement of Dental Implants," 2007, https://www.researchgate.net/publication/26524283.

10. S. Du, K. Zhang, M. Wen, et al., "Optimizing the Tribological Behavior of Tantalum Carbide Coating for the Bearing in Total Hip Joint Replacement," *Vacuum* 150 (2018): 222–231, https://doi.org/10.1016/j.vacuum.2018.01.050.

11. M. Marasy Dewidar, H.-C. Yoon, and J. K. Lim, "Mechanical Properties of Metals for Biomedical Applications Using Powder Metallurgy Process: A Review," *Metals and Materials International* 12 (2006): 193–206.

12. Z. A. Uwais, M. A. Hussein, M. A. Samad, and N. Al-Aqeeli, "Surface Modification of Metallic Biomaterials for Better Tribological Properties: A Review," *Arabian Journal for Science and Engineering* 4211 (2017): 4493–4512.

13. L. Kunčická, R. Kocich, and T. C. Lowe, "Advances in Metals and Alloys for Joint Replacement," *Progress in Materials Science* 88 (2017): 232–280.

14. P. M. Hashemi, E. Borhani, and M. S. Nourbakhsh, "A Review on Nanostructured Stainless-Steel Implants for Biomedical Application," *Nanomedical Journal* 3, no. 4 (2016): 202–216, https://doi.org/10.22038/nmj.2016.7574.

15. R. A. Antunes, N. B. De Lima, M. De Almeida Rizzutto, O. Z. Higa, M. Saiki, and I. Costa, "Surface Interactions of a W-DLC-Coated Biomedical AISI 316L Stainless Steel in Physiological Solution," *Journal of Materials Science: Materials in Medicine* 24, no. 4 (2013): 863–876, https://doi.org/10.1007/s10856-013-4871-z.

16. A. Büyüksağiş, E. Bulut, and Y. Kayalı, "Corrosion Behaviors of Hydroxyapatite Coated by Electrodeposition Method of Ti6Al4V, Ti and AISI 316L SS Substrates," *Protection of Metals and Physical Chemistry of Surfaces* 49, no. 6 (2013): 776–787, https://doi.org/10.1134/S207020511306018X.

17. G. E. Novikova, "Introduction to Corrosion of Bioimplants," *Protection of Metals and Physical Chemistry of Surfaces* 47, no. 3 (2011): 372–380, https://doi.org/10.1134/S2070205111030105.

18. K.-K. Chew, S. H. S. Zein, and A. L. Ahmad, "The Corrosion Scenario in Human Body: Stainless Steel 316L Orthopaedic Implants," *Natural Science* 4, no. 3 (2012): 184–188, https://doi.org/10.4236/ns.2012.43027.

19. D. Jaiswal, V. Singh, D. Pathote, and C. K. Behera, "Electrochemical Behaviour of Lead-Free Sn–0.7Cu–xIn Solders Alloys in 3.5 Wt% NaCl Solution," *Journal of Materials Science: Materials in Electronics* 32, no. 18 (2021): 23371–23384, https://doi.org/10.1007/s10854-021-06824-3.

20. D. Pathote, D. Jaiswal, V. Singh, and C. K. Behera, "Optimization of Electrochemical Corrosion Behavior of 316L Stainless Steel as an

Effective Biomaterial for Orthopedic Applications," *Materials Today: Proceedings* 57 (2022): 265–269, https://doi.org/10.1016/j.matpr.2022.02.501.

21. K.-K. Chew, S. H. S. Zein, and A. L. Ahmad, "The Corrosion Scenario in Human Body: Stainless Steel 316L Orthopaedic Implants," *Natural Science* 4, no. 3 (2012): 184–188, https://doi.org/10.4236/ns.2012.43027.

22. D. Jaiswal, D. Pathote, V. Singh, and C. K. Behera, "Electrochemical Behaviour of Lead-Free Sn-In-Al Solders Alloys in 3.5 Wt.% Nacl Solution," *Materials Today: Proceedings* 57 (2022): 187–193, https://doi.org/10.1016/j.matpr.2022.02.315.

23. D. Pathote, D. Jaiswal, V. Singh, and C. K. Behera, "Electrochemical Corrosion Behavior of Tantalum Coated 316L Stainless Steel by DC Magnetron Sputtering for Orthopedic Applications," *Applied Surface Science Advances* 13 (2023): 100365, https://doi.org/10.1016/j.apsadv.2022.100365.

24. D. Pathote, P. Kumari, V. Singh, D. Jaiswal, R. K. Gautam, and C. K. Behera, "Biocompatibility Evaluation, Wettability, and Scratch Behavior of Ta-Coated 316L Stainless Steel by DC Magnetron Sputtering for the Orthopedic Applications," *Surface and Coatings Technology* 459 (2023): 129392.

25. D. Pathote, D. Jaiswal, V. Singh, R. K. Gautam, and C. K. Behera, "Wear Behavior and Microhardness Studies of Tantalum (Ta)-Coated 316L Stainless Steel by DC Magnetron Sputtering for the Orthopedic Applications," *Journal of Materials Science* 57, no. 45 (2022): 21039–21056, https://doi.org/10.1007/s10853-022-07939-6.

26. A. Parsapour, S. N. Khorasani, and M. H. Fathi, "Corrosion Behavior and Biocompatibility of Hydroxyapatite Coating on H_2SO_4 Passivated 316L SS for Human Body Implant," *Acta Metallurgica Sinica (English Letters)* 26 (2013): 409–415.

27. Z. Wang, Z. Q. Zhou, L. Zhang, J. Y. Hu, Z. R. Zhang, and M. X. Lu, "Effect of pH on the Electrochemical Behaviour and Passive Film Composition of 316L Stainless Steel," *Acta Metallurgica Sinica* 32 (2019): 585–598.

28. D. B. Kumar, R. Nagalakshmi, K. G. Muthurajan, V. Rajasekar, and S. Parthasarathi, "Corrosion Behaviour of SS 316L in Different Medium," *Journal of Chemical and Pharmaceutical Research* 9, no. 9 (2015): 284–286.

29. G. E. Novikova, "Introduction to Corrosion of Bioimplants," *Protection of Metals and Physical Chemistry of Surfaces* 47, no. 3 (2011): 372–380.

30. R. Alias, R. Mahmoodian, K. Genasan, K. M. Vellasamy, M. Hamdi Abd Shukor, and T. Kamarul, "Mechanical, Antibacterial, and Biocompatibility Mechanism of PVD Grown Silver–Tantalum-Oxide-Based Nanostructured Thin Film on Stainless Steel 316L for Surgical Applications," *Materials Science and Engineering: C* 107 (2020): 110304.

31. G. Manivasagam, D. Dhinasekaran, and A. Rajamanickam, "Biomedical Implants: Corrosion and Its Prevention-A Review," *Recent Patents on Corrosion Science* 2, no. 1 (2010): 40–54.

32. C. Schille, M. Braun, H. P. Wendel, et al., "Corrosion of Experimental Magnesium Alloys in Blood and PBS: A Gravimetric and Microscopic Evaluation," *Materials Science and Engineering: B* 176, no. 20 (2011): 1797–1801.

33. L. Geyao, D. Yang, C. Wanglin, and W. Chengyong, "Development and Application of Physical Vapor Deposited Coatings for Medical Devices: A Review," *Procedia CIRP* 89 (2020): 250–262, https://doi.org/10.1016/j.procir.2020.05.149.

34. M. Talha, C. K. Behera, S. Kumar, O. Pal, G. Singh, and O. P. Sinha, "Long-Term and Electrochemical Corrosion Investigation of Cold-Worked AISI 316L and 316LVM Stainless Steels in Simulated Body Fluid," *RSC Advances* 4, no. 26 (2014): 13340–13349.

35. J. C. E. Odekerken, T. J. M. Welting, J. J. C. Arts, and G. Walenkamp, "Modern Orthopaedic Implant Coatings — Their Pro's, Con's and Evaluation Methods," in *Modern Surface Engineering Treatments*, ed. M. Aliofkhazraei (InTech, 2013).

36. P. Mahmoudi Hashemi, E. Borhani, and M. S. Nourbakhsh, "A Review on Nanostructured Stainless-Steel Implants for Biomedical Application," *Nanomedicine Journal* 3, no. 4 (2016): 202–216, http://nmj.mums.ac.ir/article_7574.html%0Ahttp://nmj.mums.ac.ir/article_7574_5c59f5d2fd08d4b425c231704a4a388e.pdf.

37. N. Hassan and N. A. Abdel Ghany, "Corrosion of Biomaterials: Anodic Treatment and Evaluation of 316L Stainless Steel in Simulated Body Fluid," *Corrosion Engineering, Science and Technology* 52, no. 4 (2017): 267–275, https://doi.org/10.1080/1478422X.2016.1267932.

38. D. D. Kumar and G. S. Kaliaraj, "Multifunctional Zirconium Nitride/Copper Multilayer Coatings on Medical Grade 316L SS and Titanium Substrates for Biomedical Applications," *Journal of the Mechanical Behavior of Biomedical Materials* 77 (2018): 106–115, https://doi.org/10.1016/j.jmbbm.2017.09.007.

39. G. A. Santos, "The Importance of Metallic Materials as Biomaterials," *Advances in Tissue Engineering & Regenerative Medicine: Open Access* 3, no. 1 (2017): 300–302.

40. A. Bekmurzayeva, W. J. Duncanson, H. S. Azevedo, and D. Kanayeva, "Surface Modification of Stainless Steel for Biomedical Applications: Revisiting a Century-Old Material," *Materials Science and Engineering: C* 93 (2018): 1073–1089, https://doi.org/10.1016/j.msec.2018.08.049.

41. A. Samanta, R. Rane, B. Kundu, et al., "Bio-Tribological Response of Duplex Surface Engineered SS316L for Hip Implant Application," *Applied Surface Science* 507 (2020): 145009, https://doi.org/10.1016/j.apsusc.2019.145009.

42. M. H. Nie, P. F. Jiang, Y. X. Zhou, Y. L. Li, and Z. H. Zhang, "Studies on the 316/NiTi Functionally Gradient Ultra-Thick Coatings Fabricated With Directed Energy Deposition: Microstructure, Crystallography and Wear Mechanism," *Applied Surface Science* 630 (2023): 157497, https://doi.org/10.1016/j.apsusc.2023.157497.

43. A. Samanta, R. Rane, B. Kundu, et al., "Bio-Tribological Response of Duplex Surface Engineered SS316L for Hip-Implant Application," *Applied Surface Science* 507 (2020): 145009, https://doi.org/10.1016/j.apsusc.2019.145009.

44. P. Trzaskowska, E. Rybak, K. Jabłońska-Ławniczak, et al., "The Potential of Electropolymerized Crosslinked Pegdma Coating on Steel for Further Functionalization: Surface Parameters and HMEC-1 Cells Attachment Correlations," *Applied Surface Science* 635 (2023): 157761, https://doi.org/10.1016/j.apsusc.2023.157761.

Supporting Information

Additional supporting information can be found online in the Supporting Information section.